Key Points:
- Climate model simulations suggest a lagged response in the global growth rate of atmospheric CO_2 due to COVID-19 emissions reductions
- Detection of this reduction in observations is hampered by internal variability combined with reduced ocean and land uptake of CO_2
- Our results foreshadow the challenges of detecting the effects of CO_2 mitigation efforts to meet the Paris climate agreement

On the Detection of COVID-Driven Changes in Atmospheric Carbon Dioxide

Nicole S. Lovenduski[1] , Abhishek Chatterjee[2,3] , Neil C. Swart[4] , John C. Fyfe[4], Ralph F. Keeling[5] , and David Schimel[2]

[1]Department of Atmospheric and Oceanic Sciences and Institute of Arctic and Alpine Research, University of Colorado, Boulder, CO, USA, [2]Carbon Cycle and Ecosystems Group, Jet Propulsion Laboratory, California Institute of Technology, Pasadena, CA, USA, [3]USRA/NASA Goddard Space Flight Center, Greenbelt, MD, USA, [4]Canadian Centre for Climate Modelling and Analysis, Environment and Climate Change Canada, Victoria, BC, Canada, [5]Scripps Institution of Oceanography, University of California San Diego, La Jolla, CA, USA

Abstract We assess the detectability of COVID-like emissions reductions in global atmospheric CO_2 concentrations using a suite of large ensembles conducted with an Earth system model. We find a unique fingerprint of COVID in the simulated growth rate of CO_2 sampled at the locations of surface measurement sites. Negative anomalies in growth rates persist from January 2020 through December 2021, reaching a maximum in February 2021. However, this fingerprint is not formally detectable unless we force the model with unrealistically large emissions reductions (2 or 4 times the observed reductions). Internal variability and carbon-concentration feedbacks obscure the detectability of short-term emission reductions in atmospheric CO_2. COVID-driven changes in the simulated, column-averaged dry air mole fractions of CO_2 are eclipsed by large internal variability. Carbon-concentration feedbacks begin to operate almost immediately after the emissions reduction; these feedbacks reduce the emissions-driven signal in the atmosphere carbon reservoir and further confound signal detection.

Plain Language Summary COVID pandemic lockdowns suddenly slowed the rate at which we burned fossil fuels and released carbon dioxide into the atmosphere, yet we cannot find any significant reductions in the growth of carbon dioxide in the atmosphere from our measurements. Here we provide some reasons to explain this conundrum. We use a climate model to mimic the changes in atmospheric carbon that would occur with different amounts of reductions in fossil fuel burning. We find that it is hard to see the change in fossil fuel burning in atmospheric carbon dioxide or its growth because of a large background component of natural variability. In addition, once we reduce our fossil fuel burning and the amount of carbon dioxide in the atmosphere decreases, the ocean and land also stop taking up as much carbon as normal. As we will soon lower our fossil fuel burning on purpose to slow climate change, our findings forewarn of the difficulties of detecting the effects of this in measurements of atmospheric carbon dioxide.

1. Introduction

Falling energy demand during the COVID-19 pandemic led to rapid decreases in energy-related carbon dioxide (CO_2) emissions. In 2020, global annual CO_2 emissions fell by 7% to 2011 levels (9.3 Pg C yr^{-1}; Friedlingstein et al., 2020), and the rapid decline in emissions during the first half of 2020 surpassed the rate of emission declines during any previous economic recession or World War II (Forster et al., 2020; Friedlingstein et al., 2020; Le Quéré et al., 2020; Liu et al., 2020). Global annual CO_2 emissions are forecast to remain below 2019 levels through 2021, and subsequent recovery of emissions is expected within a few years (International Energy Agency, 2021; Le Quéré et al., 2021). The precipitous and short-lived drop in emissions during the COVID pandemic offers a unique opportunity to assess the detection of these types of emissions declines in observations of the global carbon cycle.

While the COVID-related CO_2 emissions reductions had a measurable impact on regional atmospheric CO_2 concentrations (Buchwitz et al., 2021; Chevallier et al., 2020; Liu et al., 2021; Tohjima et al., 2020; Turner et al., 2020; Weir et al., 2020; Wu et al., 2021), as of this writing, there is no indication of a global-scale decrease in the atmospheric CO_2 mixing ratio or its growth rate due to the emissions reductions (NOAA

Global Monitoring Laboratory, 2021; World Meteorological Organization, 2020). Even with a robust global measurement system, the detection of COVID-related emissions reductions in global CO_2 or its growth rate is challenging due to two factors: (1) internal variability in the climate system and (2) carbon-concentration feedbacks. Internal variability is unforced climate variability that arises from the coupled interactions of the atmosphere and ocean (e.g., El Niño-Southern Oscillation (ENSO); Deser, Phillips, et al., 2012). The role of internal variability in the growth rate of CO_2 has been well documented in the literature (e.g., Frölicher et al., 2013; Keeling et al., 2001; Sarmiento & Gruber, 2002), and multiple studies implicate this variability in our inability to detect emissions changes in measurements of atmospheric CO_2 (e.g., Peters et al., 2017). Carbon-concentration feedbacks manifest from the sensitivity of the ocean and land carbon reservoirs to changing CO_2 (Arora et al., 2013, 2020; Friedlingstein et al., 2006). Recent studies suggest that the ocean carbon reservoir rapidly responds to perturbations in CO_2 (McKinley et al., 2020; Ridge & McKinley, 2021), and this can further confound the detection of emissions changes in measurements of atmospheric CO_2. It is critical that we develop a deeper understanding of the role of internal variability and carbon feedbacks on the detectability of emissions changes to inform both near-term (1–10 years) predictions of the carbon cycle (Ilyina et al., 2021) and the verification of future emissions reductions (Peters et al., 2017; Ridge & McKinley, 2021).

Initial-condition large ensembles of Earth system models are a relatively new tool that provides a means to quantify the anthropogenic influence on the Earth system in the presence of internal climate variability (Deser et al., 2020). These large ensembles are a set of simulations with a single Earth system model: each simulation or ensemble member is initialized slightly differently to create diverging climate trajectories, while all ensemble members are externally forced with a common emission scenario (Deser, Knutti, et al., 2012). Multiple studies have used large ensembles to account for the role of internal variability in long-term climate trends (e.g., Deser, Phillips, et al., 2012, 2016). Most recently, large ensembles have been used to estimate the anthropogenic influence on short-term climate signals (such as for the COVID pandemic, see, e.g., Fyfe et al., 2021; Gettelman et al., 2021; Jones et al., 2021), and to make Earth system predictions over the near-term (1–10 years; Yeager et al., 2018). However, no studies have used a large ensemble framework to assess the detectability of short-term CO_2 emissions reductions from atmospheric CO_2 measurements.

Here, we develop an understanding of the role of internal variability and carbon feedbacks on the detectability of a short-lived CO_2 emissions reduction in the atmospheric mixing ratio of CO_2 (χCO_2) using output from an initial-condition large ensemble of an Earth system model. This 30-member ensemble evolves the Earth system under three, short-term emissions reduction scenarios of differing magnitudes. We investigate the detectability of the emissions reduction using several modeled parameters that characterize atmospheric CO_2: the χCO_2 growth rate, the column-averaged CO_2(XCO$_2$), and the integrated atmospheric carbon reservoir.

2. Methods

We utilize the Canadian Earth System Model version 5 (CanESM5), which consists of coupled atmosphere, ocean, sea-ice, land surface, and land/ocean carbon cycle model components (Swart et al., 2019). The atmospheric model in CanESM5 is version five of the Canadian Atmospheric Model (CanAM5) that has an approximate 2.8° horizontal resolution and 49 vertical levels of varying thickness on a hybrid sigma-pressure vertical grid and similar physical parameterizations as its predecessor (CanAM4; Swart et al., 2019). The land component of CanESM5 consists of the Canadian Land Surface Scheme (CLASS) and the Canadian Terrestrial Ecosystem Model (CTEM) that produce fluxes of energy, water, and carbon dioxide at the land-atmosphere interface via the simulation of physical and biogeochemical processes, including the CO_2 fertilization of photosynthesis (Swart et al., 2019). The ocean physical and biogeochemical components of CanESM5 used in this study are the CanNEMO physical model coupled to the Canadian Model of Ocean Carbon (CMOC), which simulates ocean carbon and its exchange with the atmosphere at approximately 1° horizontal resolution (Swart et al., 2019). In our study, the concentration of CO_2 in the CanESM5 atmosphere is modeled as a three-dimensional, prognostic passive tracer that responds to air-sea and air-land CO_2 fluxes from the coupled land and ocean carbon cycle components, and to specified CO_2 emissions.

We analyze output from five ensembles of CanESM5. In each case, ensemble members are initialized with slightly perturbed climate states to simulate a range of internal variability, but each member in a given ensemble experiences identical external forcing. The first ensemble (the historical ensemble) covers the period from 1850 to 2014 and consists of nine ensemble members of CanESM5 forced with a global historical emission data set of CO_2 and other climate-relevant gases and aerosols—this was devised for emissions-driven historical simulations in Phase 6 of the Coupled Model Intercomparison Project (CMIP6; Figure S1a in Supporting Information S1; Hoesly et al., 2018). The second ensemble (the control ensemble) covers the period 2015–2100 and consists of 30 ensemble members of CanESM5 integrated under the ESM-SSP2-4.5 emissions scenario (Figure S1b in Supporting Information S1; O'Neill et al., 2016). The remaining 3 ensembles span 2019–2040 and consist of 30 members each that are forced with COVID-like CO_2 emissions reductions beginning in December 2019 and resolving in December 2021; peak emissions reductions of 25% (COVID-like), 50% ($2 \times$ COVID-like), and 100% ($4 \times$ COVID-like) occur in May 2020 (Figure S1b in Supporting Information S1). Hereafter, we refer to these later three ensembles collectively as the CanESM5-COVID ensemble, as described in Fyfe et al. (2021) and Lovenduski et al. (2021). The CO_2 emissions in the historical and control ensembles have spatial and seasonal variability; emissions are highest near urban centers in the Northern Hemisphere (Figure S2a in Supporting Information S1) and peak in boreal winter when energy consumption in the Northern Hemisphere is at a maximum (Figure S2b in Supporting Information S1). Emissions are scaled uniformly for the COVID ensembles to maintain this spatial and seasonal variability. In the CanESM5-COVID ensemble output we analyze here, emissions of CO_2 from other sources (e.g., land use change) and emissions of other climate relevant gases and aerosols are prescribed from the ESM-SSP2-4.5 scenario, that is, these emissions do not change due to COVID.

The global carbon cycle in CanESM5 compares well with observational metrics and is thus an appropriate tool for the study of the detectability of short-term emissions reductions in atmospheric χCO_2. Air-sea and air-land CO_2 fluxes from the historical simulation of CanESM5 were previously evaluated in Swart et al. (2019). Briefly, Swart et al. (2019) illustrate high skill and low root mean square error between simulated and observed spatial patterns of Gross Primary Production (GPP) and air-sea CO_2 flux over 1981 to 2010. CanESM5 tends to overestimate GPP in sub-saharan Africa and underestimate GPP in the Amazon rainforest, likely due to precipitation biases (Swart et al., 2019). Historical CanESM5 air-sea CO_2 fluxes are biased high in the North Atlantic and low in the Southern Ocean, such that the globally integrated air-sea CO_2 flux exhibits little bias as compared to observations (Swart et al., 2019). CanESM5 captures the broad features of the amplitude and phasing of the seasonal cycle of χCO_2 measured at Barrow (BRW), Mauna Loa (MLO), and South Pole (SPO), though the seasonal drawdown of CO_2 occurs too early at Point Barrow, and the amplitude is biased high at Mauna Loa (Figure S3 in Supporting Information S1; the model is sampled at the approximate latitude, longitude, and height of the flask sample in the real world). The de-trended interhemispheric gradient in observed, annual mean χCO_2 exhibits large annual-to-decadal fluctuations over 1960–2020 that are generally replicated by the model (Figure S4 in Supporting Information S1). The de-trended interhemispheric difference in the CanESM5 historical ensemble members encapsulate the observations and the ensemble mean replicates the decadal variations in the observations, though the interannual variance of individual ensemble members is greater than that of the observational record (Figure S4 in Supporting Information S1). Finally, the CanESM5 control ensemble mean exhibits a similar growth rate in χCO_2 (2.4 ppm yr^{-1} over 2015–2019; see Figure 1) as calculated from observations (2.57 $\pm$ 0.08 ppm yr^{-1} over 2015–2019; https://gml.noaa.gov/ccgg/trends/gl_gr.html). The actual growth rate derived from observations is slightly higher due to the impact of the 2015–2016 El Niño event on the carbon cycle (Chatterjee et al., 2017; Liu et al., 2017).

3. Results

The 30-member CanESM5 COVID ensemble predicts a decrease in the de-seasoned, monthly growth rate of χCO_2 from January 2020 through February 2021, followed by an increase in growth rate from February through December 2021 under all of the COVID emission scenarios when sampled at both Mauna Loa and 12 global flask sites (Figure 1; growth rate is calculated as the difference in χCO_2 for a given month relative to the same month in the previous year; flask sites as in Cadule et al., 2010). The decrease in the growth rate is largest for the $4 \times$ COVID-like emissions scenario and smallest for the COVID-like emissions scenario
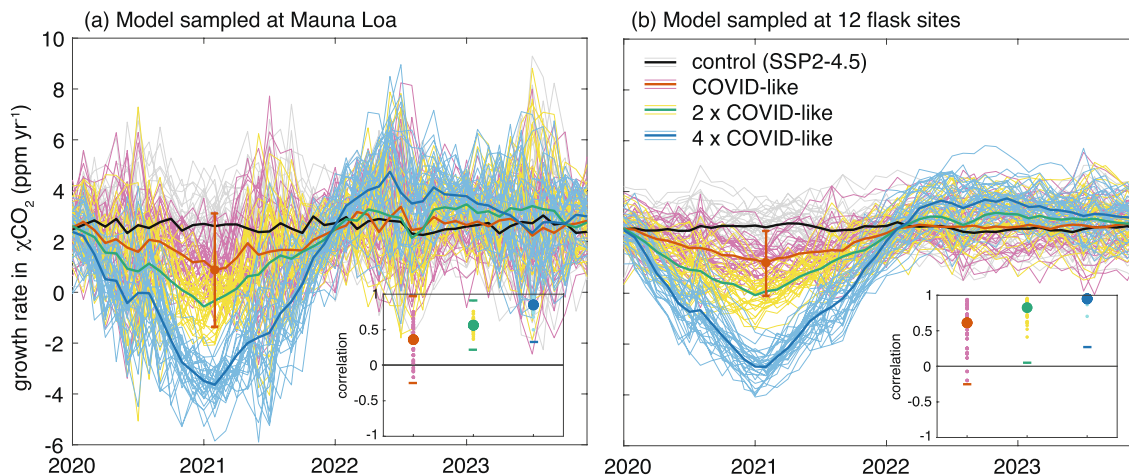
Figure 1. Temporal evolution of the growth rate of de-seasoned, monthly χCO_2 from the CanESM5 COVID ensemble sampled at (a) Mauna Loa, and (b) the average of 12 flask sites (as in Cadule et al., 2010) over 2020–2024. Growth rate is calculated as the difference in χCO_2 for a given month relative to the same month in the previous year. Thin lines show individual ensemble members, and thick lines show the ensemble mean for each emissions scenario. Red dot and range illustrates the mean and 2σ (95%) confidence interval in February 2021 for the COVID-like emissions scenario. Subplots show the temporal correlation coefficients of individual ensemble members with the ensemble mean over Jan 2020–Dec 2021 for each emissions scenario. Small circles show the correlation coefficients across the 30 ensemble members, large circles show the mean correlation coefficients, and dashes indicate 2σ (95%) confidence intervals.

and peaks in February 2021 under all COVID scenarios (Figure 1). Meanwhile, the control ensemble exhibits little change in its growth rate over this period (Figure 1). This suggests that the χCO_2 growth rate is highly sensitive to the magnitude of the emissions reduction, and that growth rate anomalies at Mauna Loa and across the global flask network tend to be largest ~9 months after the peak emissions reduction (May 2020; Figure S1b in Supporting Information S1). This delay is consistent with the global mixing timescale for CO_2 in the atmosphere (Forster et al., 2007). Under the $4 \times$ COVID-like scenario, the growth rate exceeds the control growth rate from 2022 through 2024 before returning to control values (Figure 1). Figure 1 also reveals that internal variability tends to obscure the emissions reduction signal in χCO_2 at an individual site more than in the global average (cf. Figures 1a and 1b); averaging across multiple sites tends to dampen the effects of internal variability that manifest most strongly at local and regional scales (Hawkins & Sutton, 2009). As a result, the ensemble-mean February 2021 COVID-like χCO_2 growth rate is significantly different from the control ensemble mean in the average of the 12 flask sites, but not at Mauna Loa (Figure 1; significance calculated using a 2σ (95%) confidence interval across the COVID-like ensemble members). If we wish to detect a signal of the COVID-driven emissions reduction in the real-world growth rate of χCO_2, our modeling study suggests that we are most likely to find it in early 2021 by averaging across measurements collected in the global flask network.

Is it possible to detect the change in the de-seasoned, monthly χCO_2 growth rate from flask observations in the real world, where we have only a single "ensemble member"? To answer this question, we turn to a formal statistical detection framework, where we use the unique ensemble mean "fingerprint" of the growth rate in the model sampled at flask sites (i.e., the V-shaped dip and recovery in the ensemble-mean growth rate over January 2020 to December 2021 in Figure 1) and quantify the correlation of each individual ensemble member with this fingerprint for each emissions scenario. This statistical detection approach for hypothetical observations (we haven't yet measured the growth rate in December 2021, for example) is identical to the one outlined in Lovenduski et al. (2021) and mimics the approach for the detection of a climate change signal in real-world observations (Bindoff & Stott, 2013). The resulting correlation coefficients are shown in the subplots of Figure 1, where small circles show the set of 30 Pearson's correlation coefficients (r) with the ensemble mean fingerprint across the 30 ensemble members, and large circles show the mean correlation coefficients (calculated using a Fisher's z transform; see Lovenduski et al., 2021) for each COVID-like emissions scenario. For the model sampled at Mauna Loa, the mean correlation coefficient for the COVID-like ensemble is 0.4 with a wide range; stronger emissions reductions increase the mean correlation coefficient and narrow the range (subplot in Figure 1a), suggesting a higher probability of detecting the fingerprint from a single ensemble member or hypothetical observational record under higher emissions
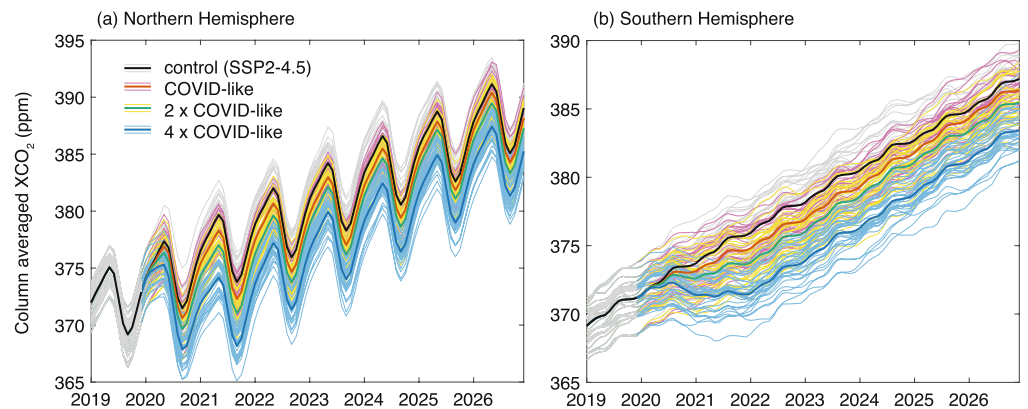
Figure 2. Temporal evolution of monthly, column-averaged χCO_2 over (a) the Northern Hemisphere, 20°N–55°N, and (b) the Southern Hemisphere, 20°S-55°S, simulated with the CanESM5 COVID ensemble. Thin lines show individual ensemble members, and thick lines show the ensemble mean for each emissions scenario.

reductions. Indeed, the range of correlation coefficients is only statistically different from zero (using a 2σ/95% confidence interval) under the $2 \times$ COVID-like and $4 \times$ COVID-like emission scenarios (subplot in Figure 1a), indicating that significant detection of the COVID fingerprint is only possible in cases with more extreme emissions reductions than those that occurred during the COVID pandemic. Similar patterns are observed when the model is sampled at 12 flask sites (Figure 1b), though the correlations are overall higher due to reduced internal variability.

Model-estimated, column-averaged dry-air mole fraction of χCO_2 (referred to as XCO_2 by the satellite community; Crisp et al., 2004) averaged over the extratropical Northern and Southern Hemispheres (20°N–55°N and 20°S–55°S, respectively) shows only a small signal of COVID-like emissions reductions amid large internal variability (Figure 2). While the emissions reduction signal is more pronounced in the Southern Hemisphere extratropics, there is large overlap of the various model ensemble members from the various emission scenarios (Figure 2b), and only the $4 \times$ COVID-like ensemble mean is significantly different from the control ensemble mean at the 2σ (95%) level (not shown). The vertical integration of the atmospheric column and the diffusive nature of atmospheric transport makes the modeled column concentrations less sensitive to changes in the surface emissions signal (Miller et al., 2007; Rayner & O'Brien, 2001), thus making the signal more difficult to detect in the column.

Carbon-concentration feedbacks further obscure the detection of COVID emissions reductions in the atmospheric carbon reservoir. Figure 3 shows the anomaly in the ensemble-mean cumulative change in the modeled atmosphere, ocean, and land carbon reservoirs from December 2019 to December 2040, where the anomaly is calculated relative to the control ensemble mean. In the atmosphere, the cumulative reservoir anomaly is negative for the duration of the simulations regardless of emissions scenario (Figure 3a), indicating that each of the COVID-like emissions perturbations leads to a forced change in the cumulative atmospheric reservoir lasting well beyond the emissions recovery in 2022 (cf. Figures 3a and S1b). For both the $2 \times$ COVID-like and $4 \times$ COVID-like scenarios, the atmosphere reservoir anomaly falls outside of the ensemble spread due to internal variability (gray shading) for several years. Meanwhile, the ocean and land carbon reservoirs also respond to the COVID-like emissions reductions, the ocean carbon sink immediately slows with decreasing χCO_2 under all COVID-like scenarios (Figure 3b; Lovenduski et al., 2021), and the land carbon sink also weakens, most noticeably under the $2 \times$ COVID-like and $4\times$ COVID-like scenarios (Figure 3c). The ocean reservoir anomaly falls outside of the spread due to internal variability only in the $2 \times$ COVID-like and $4 \times$ COVID-like scenarios (Figure 3b; Lovenduski et al., 2021). The land carbon sink anomaly is fully within the internal variability bounds (Figure 3c), due to high internal variability in the land-air CO_2 flux (Denman et al., 2007). Nevertheless, these results suggest that COVID emissions reductions cause both the ocean and land to absorb less carbon than usual in our model, thus reducing the perturbation in the atmosphere. To illustrate this point further, we estimate the ensemble-mean, cumulative change in the atmospheric carbon reservoir due only to emissions changes and plot the resulting reservoir anomaly as dashed lines in Figure 3a. This illustration reveals a critical role for carbon-concentration feedbacks in the
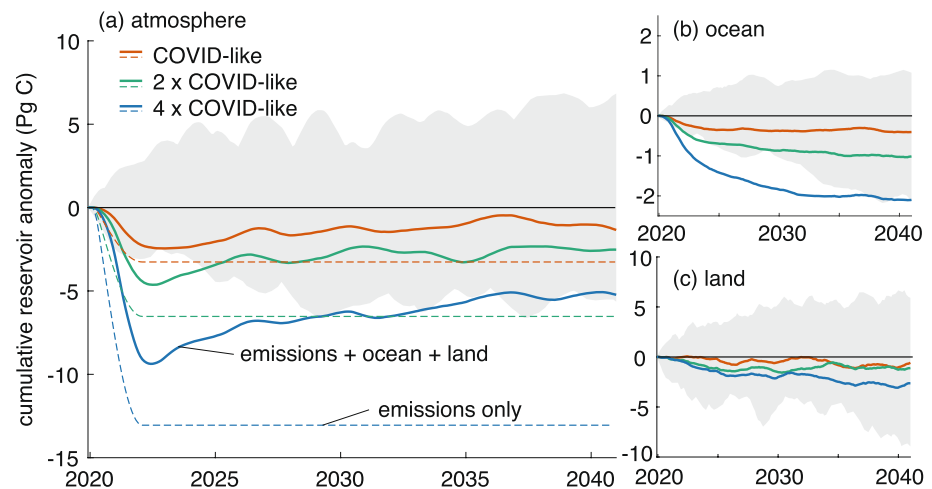
Figure 3. Cumulative changes in the (a) atmosphere, (b) ocean, and (c) land carbon reservoirs from December 2019 onwards, as simulated by the CanESM5 COVID ensemble. Colored lines show the anomaly in the ensemble-mean reservoir size relative to the control ensemble mean (SSP2-4.5), and gray shading indicates the spread in the cumulative reservoir anomaly across the control ensemble. Dashed lines in (a) show the cumulative changes in atmospheric carbon due to anomalous emissions alone.

detection of COVID-driven emissions reductions: if not for the slowing ocean and land carbon sinks, the COVID-like emissions reduction signal in the atmospheric carbon reservoir would have been detectable above the noise of internal variability for three consecutive years (2022–2025), and for longer durations with larger emission perturbations (Figure 3a).

4. Conclusions and Discussion

We use an initial-condition large ensemble of an Earth system model to assess the detectability of the COVID-driven emissions reductions signal in measurements of atmospheric CO_2 above the noise of internal variability and carbon-concentration feedbacks. We find a unique fingerprint in atmospheric CO_2 growth rates calculated from simulated χCO_2 measurements under COVID-like emissions reductions. The largest negative anomalies in the atmospheric χCO_2 growth rate appear in February 2021, ~9 months after the peak emissions reductions. This growth rate signal is more likely to be detected above the noise of internal variability when averaging over global flask network sites, rather than at an individual site. However, this unique fingerprint is not formally detectable using a climate signal detection statistical approach, unless we force the model with unrealistically large emissions reductions. Internal variability obscures the detection of change in the interhemispheric difference of simulated χCO_2 from flask measurements and the simulated extra-tropical column-average XCO_2 from satellite observations. Carbon-concentration feedbacks further reduce the emissions signal in the atmospheric carbon reservoir. When we remove the effects of these feedbacks on the atmospheric carbon reservoir, the signal in the cumulative reservoir anomaly is detectable above the noise of internal variability over a three consecutive year period (2022–2025).

Our study illuminates the challenges associated with detecting brief CO_2 emissions reductions in global-scale atmospheric CO_2 from our established observational measurement systems. In order to see the emergence of the signal of COVID-driven emissions reductions in atmospheric CO_2, one needs to first remove the influence of internal climate variability and carbon-concentration feedbacks from the atmospheric CO_2 measurements. While we are getting closer to quantifying the internal contribution to the total signal from our measurements and producing near-real time estimates of this variability (e.g., Betts et al., 2016, 2020), we are not yet capable of quantifying carbon feedbacks from our current, exploratory observational system (e.g., Sellers et al., 2018). Further, the ocean and terrestrial carbon reservoirs are only sparsely observed and, with the exception of a few surface ocean buoys that measure ocean CO_2 partial pressure (Sutton et al., 2019), the high-quality estimates of changing air-sea and air-land CO_2 fluxes that are available in a historical context are not yet available in near-real time due to the high costs of fast data

dissemination and other impediments. As we move into a world characterized by intentional emissions reductions associated with international climate change mitigation policies, we should consider this measurement infrastructure in the ocean and terrestrial biosphere to detect the signal and monitor the impact of intentional emissions reductions in atmospheric CO_2.

Data Availability Statement

The data from the CanESM5 simulations used in this study are published through the Government of Canada Open Data Portal, and can be accessed at http://crd-data-donnees-rdc.ec.gc.ca/CCCMA/publications/COVID19/. The χCO_2 flask data are from the Scripps CO_2 program, and can be accessed at https://scrippsco2.ucsd.edu/data/atmospheric_co2/sampling_stations.html.

References

Arora, V. K., Boer, G. J., Friedlingstein, P., Eby, M., Jones, C. D., Christian, J. R., et al. (2013). Carbon–concentration and carbon–climate feedbacks in CMIP5 Earth System Models. *Journal of Climate*, *26*(15), 5289–5314. https://doi.org/10.1175/JCLI-D-12-00494.1

Arora, V. K., Katavouta, A., Williams, R. G., Jones, C. D., Brovkin, V., Friedlingstein, P., et al. (2020). Carbon–concentration and carbon–climate feedbacks in CMIP6 models and their comparison to CMIP5 models. *Biogeosciences*, *17*(16), 4173–4222. https://doi.org/10.5194/bg-17-4173-2020

Betts, R., Jones, C., Jin, Y., Keeling, R., Kennedy, J., Knight, J., & Scaife, A. (2020). Analysis: What impact will the coronavirus pandemic have on atmospheric CO_2? *CarbonBrief*. Retrieved from https://www.carbonbrief.org/analysis-what-impact-will-the-coronavirus-pandemic-have-on-atmospheric-co2

Betts, R. A., Jones, C. D., Knight, J. R., Keeling, R. F., & Kennedy, J. J. (2016). El Niño and a record CO_2 rise. *Nature Climate Change*, *6*, 806–810. https://doi.org/10.1038/nclimate3063

Bindoff, N. L., & Stott, P. A. (2013). Chapter 10: Detection and attribution of climate change: From global to regional. In T. F. Stocker, D. Qin, G.-K. Plattner, M. M. B. Tignor, S. K. Allen, J. Boschung, et al. (Eds.), *Climate change 2013: The physical Science Basis. Contribution of Working Group I to the Fifth Assessment Report of the Intergovernmental Panel on Climate Change* (p. 1535). Cambridge, United Kingdom and New York, NY, USA: Cambridge University Press.

Buchwitz, M., Reuter, M., Noël, S., Bramstedt, K., Schneising, O., Hilker, M., et al. (2021). Can a regional-scale reduction of atmospheric CO_2 during the COVID-19 pandemic be detected from space? A case study for East China using satellite XCO$_2$ retrievals. *Atmospheric Measurement Techniques*, *14*(3), 2141–2166. https://doi.org/10.5194/amt-14-2141-2021

Cadule, P., Friedlingstein, P., Bopp, L., Sitch, S., Jones, C. D., Ciais, P., et al. (2010). Benchmarking coupled climate-carbon models against long-term atmospheric CO_2 measurements. *Global Biogeochemical Cycles*, *24*(2). https://doi.org/10.1029/2009GB003556

Chatterjee, A., Gierach, M. M., Sutton, A. J., Feely, R. A., Crisp, D., Eldering, A., et al. (2017). Influence of El Niño on atmospheric CO_2 over the tropical Pacific Ocean: Findings from NASA's OCO-2 mission. *Science*, *358*(6360), eaam5776. https://doi.org/10.1126/science.aam5776

Chevallier, F., Zheng, B., Broquet, G., Ciais, P., Liu, Z., Davis, S. J., et al. (2020). Local anomalies in the column-averaged dry air mole fractions of carbon dioxide across the globe during the first months of the Coronavirus Recession. *Geophysical Research Letters*, *47*(22), e2020GL090244. https://doi.org/10.1029/2020GL090244

Crisp, D., Atlas, R., Breon, F.-M., Brown, L., Burrows, J., Ciais, P., et al. (2004). The Orbiting Carbon Observatory (OCO) mission. *Advances in Space Research*, *34*(4), 700–709. https://doi.org/10.1016/j.asr.2003.08.062

Denman, K. L., Brasseur, G., Chidthaisong, A., Ciais, P., Cox, P. M., Dickinson, R. E., et al. (2007). Couplings between changes in the climate system and biogeochemistry. In S. Solomon, D. Qin, M. Manning, Z. Chen, M. Marquis, K. B. Averyt, et al. (Eds.), *Climate Change 2007: The Physical Science Basis. Contribution of Working Group I to the Fourth Assessment Report of the Intergovernmental Panel on Climate Change*. Cambridge, United Kingdom and New York, NY, USA: Cambridge University Press.

Deser, C., Knutti, R., Solomon, S., & Phillips, A. S. (2012). Communication of the role of natural variability in future North American climate. *Nature Climate Change*, *2*(11), 775–779. https://doi.org/10.1038/nclimate1562

Deser, C., Lehner, F., Rodgers, K. B., Ault, T., Delworth, T. L., DiNezio, P. N., et al. (2020). Insights from Earth system model initial-condition large ensembles and future prospects. *Nature Climate Change*, *10*(4), 277–286. https://doi.org/10.1038/s41558-020-0731-2

Deser, C., Phillips, A., Bourdette, V., & Teng, H. (2012). Uncertainty in climate change projections: The role of internal variability. *Climate Dynamics*, *38*(3–4), 527–546. https://doi.org/10.1007/s00382-010-0977-x

Deser, C., Terray, L., & Phillips, A. S. (2016). Forced and internal components of winter air temperature trends over North America during the past 50 years: Mechanisms and implications. *Journal of Climate*, *6*, 2237–2258. https://doi.org/10.1175/JCLI-D-15-0304.1

Forster, P., Ramaswamy, V., Artaxo, P., Berntsen, T., Betts, R., Fahey, D. W., et al. (2007). Changes in atmospheric constituents and in radiative forcing. In S. Solomon, D. Qin, M. Manning, Z. Chen, M. Marquis, K. B. Averyt, et al. (Eds.), *Climate change 2007: The physical Science Basis. Contribution of Working Group I to the Fourth Assessment Report of the Intergovernmental Panel on climate change*. Cambridge, United Kingdom and New York, NY, USA: Cambridge University Press.

Forster, P. M., Forster, H. I., Evans, M. J., Gidden, M. J., Jones, C. D., Keller, C. A., et al. (2020). Current and future global climate impacts resulting from COVID-19. *Nature Climate Change*, *10*, 913–919. https://doi.org/10.1038/s41558-020-0883-0

Friedlingstein, P., Cox, P., Betts, R., Bopp, L., von Bloh, W., Brovkin, V., et al. (2006). Climate–carbon cycle feedback analysis: Results from the C4MIP model intercomparison. *Journal of Climate*, *19*(14), 3337–3353. https://doi.org/10.1175/JCLI3800.1

Friedlingstein, P., O'Sullivan, M., Jones, M. W., Andrew, R. M., Hauck, J., Olsen, A., et al. (2020). Global Carbon Budget 2020. *Earth System Science Data*, *12*(4), 3269–3340. https://doi.org/10.5194/essd-12-3269-2020

Frölicher, T. L., Joos, F., Raible, C. C., & Sarmiento, J. L. (2013). Atmospheric CO_2 response to volcanic eruptions: The role of ENSO, season, and variability. *Global Biogeochemical Cycles*, *27*(1), 239–251. https://doi.org/10.1002/gbc.20028

Fyfe, J. C., Kharin, V. V., Swart, N., Flato, G. M., Sigmond, M., & Gillett, N. P. (2021). Quantifying the influence of short-term emission reductions on climate. *Science Advances*, *7*(10), eabf7133. https://doi.org/10.1126/sciadv.abf7133

Gettelman, A., Lamboll, R., Bardeen, C. G., Forster, P. M., & Watson-Parris, D. (2021). Climate impacts of COVID-19 induced emission changes. *Geophysical Research Letters*, *48*(3), 805, e2020GL091. https://doi.org/10.1029/2020GL091805

Hawkins, E., & Sutton, R. (2009). The potential to narrow uncertainty in regional climate predictions. *Bulletin of the American Meteorological Society*, *90*(8), 1095–1108. https://doi.org/10.1175/2009BAMS2607.1

Hoesly, R. M., Smith, S. J., Feng, L., Klimont, Z., Janssens-Maenhout, G., Pitkanen, T., et al. (2018). Historical (1750–2014) anthropogenic emissions of reactive gases and aerosols from the Community Emissions Data System (CEDS). *Geoscientific Model Development*, *11*(1), 369–408. https://doi.org/10.5194/gmd-11-369-2018

Ilyina, T., Li, H., Spring, A., Müller, W. A., Bopp, L., Chikamoto, M. O., et al. (2021). Predictable variations of the carbon sinks and atmospheric CO_2 growth in a multi-model framework. *Geophysical Research Letters*, *48*(6), 695, e2020GL090. https://doi.org/10.1029/2020GL090695

International Energy Agency. (2021). *World energy Investment 2021, Technical Report*, IEA, Paris. Retrieved from https://www.iea.org/reports/world-energy-investment-2021

Jones, C. D., Hickman, J. E., Rumbold, S. T., Walton, J., Lamboll, R. D., Skeie, R. B., et al. (2021). The climate response to emissions reductions due to COVID-19: Initial results from CovidMIP. *Geophysical Research Letters*, *48*(8), 883, e2020GL091. https://doi.org/10.1029/2020GL091883

Keeling, C., Piper, S., Bacastow, R., Wahlen, M., Whorf, T., Heimann, M., & Meijer, H. (2001). *Exchanges of atmospheric CO_2 and $^{13}CO_2$ with the terrestrial biosphere and oceans from 1978 to 2000. I. Global aspects*. UC San Diego: Library - Scripps Digital Collection.

Le Quéré, C., Jackson, R. B., Jones, M. W., Smith, A. J. P., Abernethy, S., Andrew, R. M., et al. (2020). Temporary reduction in daily global CO_2 emissions during the COVID-19 forced confinement. *Nature Climate Change*, *10*(7), 647–653. https://doi.org/10.1038/s41558-020-0797-x

Le Quéré, C., Peters, G. P., Friedlingstein, P., Andrew, R. M., Canadell, J. G., Davis, S. J., et al. (2021). Fossil CO_2 emissions in the post-COVID-19 era. *Nature Climate Change*, *11*(3), 197–199. https://doi.org/10.1038/s41558-021-01001-0

Liu, D., Sun, W., Zeng, N., Han, P., Yao, B., Liu, Z., et al. (2021). Observed decreases in on-road CO_2 concentrations in Beijing during COVID-19 restrictions. *Atmospheric Chemistry and Physics*, *21*(6), 4599–4614. https://doi.org/10.5194/acp-21-4599-2021

Liu, J., Bowman, K. W., Schimel, D. S., Parazoo, N. C., Jiang, Z., Lee, M., et al. (2017). Contrasting carbon cycle responses of the tropical continents to the 2015–2016 El Niño. *Science*, *358*(6360), eaam5690. https://doi.org/10.1126/science.aam5690

Liu, Z., Ciais, P., Deng, Z., Lei, R., Davis, S. J., Feng, S., et al. (2020). Near-real-time monitoring of global CO_2 emissions reveals the effects of the COVID-19 pandemic. *Nature Communications*, *11*(1), 5172. https://doi.org/10.1038/s41467-020-18922-7

Lovenduski, N. S., Swart, N. C., Sutton, A. J., Fyfe, J. C., McKinley, G. A., Sabine, C., & Williams, N. L. (2021). The ocean carbon response to COVID-related emissions reductions. *Geophysical Research Letters*, *48*(6), e2020GL092263. https://doi.org/10.1029/2020GL092263

McKinley, G. A., Fay, A. R., Eddebbar, Y. A., Gloege, L., & Lovenduski, N. S. (2020). External forcing explains recent decadal variability of the ocean carbon sink. *AGU Advances*, *1*(2), e2019AV000149. https://doi.org/10.1029/2019AV000149

Miller, C. E., Crisp, D., DeCola, P. L., Olsen, S. C., Randerson, J. T., Michalak, A. M., et al. (2007). Precision requirements for space-based data. *Journal of Geophysical Research: Atmospheres*, *112*(D10). https://doi.org/10.1029/2006JD007659

NOAA Global Monitoring Laboratory. (2021). *Despite pandemic shutdowns, carbon dioxide and methane surged in 2020*. NOAA Research News. Retrieved from https://research.noaa.gov/article/ArtMID/587/ArticleID/2742/Despite-pandemic-shutdowns-carbon-dioxide-and-methane-surged-in-2020

O'Neill, B. C., Tebaldi, C., van Vuuren, D. P., Eyring, V., Friedlingstein, P., Hurtt, G., et al. (2016). The Scenario Model Intercomparison Project (ScenarioMIP) for CMIP6. *Geoscientific Model Development*, *9*(9), 3461–3482. https://doi.org/10.5194/gmd-9-3461-2016

Peters, G. P., Le Quéré, C., Andrew, R. M., Canadell, J. G., Friedlingstein, P., Ilyina, T., et al. (2017). Towards real-time verification of CO_2 emissions. *Nature Climate Change*, *7*(12), 848–850. https://doi.org/10.1038/s41558-017-0013-9

Rayner, P. J., & O'Brien, D. M. (2001). The utility of remotely sensed CO_2 concentration data in surface source inversions. *Geophysical Research Letters*, *28*(1), 175–178. https://doi.org/10.1029/2000GL011912

Ridge, S. M., & McKinley, G. A. (2021). Ocean carbon uptake under aggressive emission mitigation. *Biogeosciences*, *18*(8), 2711–2725. https://doi.org/10.5194/bg-18-2711-2021

Sarmiento, J. L., & Gruber, N. (2002). Sinks for anthropogenic carbon. *Physics Today*, *55*(8), 30–36. https://doi.org/10.1063/1.1510279

Sellers, P. J., Schimel, D. S., Moore, B., Liu, J., & Eldering, A. (2018). Observing carbon cycle–climate feedbacks from space. *Proceedings of the National Academy of Sciences*, *115*(31), 7860–7868. https://doi.org/10.1073/pnas.1716613115

Sutton, A. J., Feely, R. A., Maenner-Jones, S., Musielwicz, S., Osborne, J., Dietrich, C., et al. (2019). Autonomous seawater pCO$_2$ and pH time series from 40 surface buoys and the emergence of anthropogenic trends. *Earth System Science Data*, *11*(1), 421–439. https://doi.org/10.5194/essd-11-421-2019

Swart, N. C., Cole, J. N. S., Kharin, V. V., Lazare, M., Scinocca, J. F., Gillett, N. P., et al. (2019). The Canadian Earth System Model version 5 (CanESM5.0.3). *Geoscientific Model Development*, *12*(11), 4823–4873. https://doi.org/10.5194/gmd-12-4823-2019

Tohjima, Y., Patra, P. K., Niwa, Y., Mukai, H., Sasakawa, M., & Machida, T. (2020). Detection of fossil-fuel CO_2 plummet in China due to COVID-19 by observation at Hateruma. *Scientific Reports*, *10*(1), 18688. https://doi.org/10.1038/s41598-020-75763-6

Turner, A. J., Kim, J., Fitzmaurice, H., Newman, C., Worthington, K., Chan, K., et al. (2020). Observed impacts of COVID-19 on urban CO_2 emissions. *Geophysical Research Letters*, *47*(22), e2020GL090037. https://doi.org/10.1029/2020GL090037

Weir, B., Crisp, D., O'Dell, C., Basu, S., Chatterjee, A., Oda, T., et al. (2020). *Regional impacts of COVID-19 on carbon dioxide detected worldwide from space. arXiv*, arXiv:2011.12740.

World Meteorological Organization. (2020). Can we see the impact of COVID-19 confinement measures on CO_2 levels in the atmosphere? *WMO Greenhouse Gas Bulletin*, Number 16, 23 November 2020.

Wu, S., Zhou, W., Xiong, X., Burr, G. S., Cheng, P., Wang, P., et al. (2021). The impact of COVID-19 lockdown on atmospheric CO_2 in Xi'an, China. *Environmental Research*, *197*, 111208. https://doi.org/10.1016/j.envres.2021.111208

Yeager, S. G., Danabasoglu, G., Rosenbloom, N. A., Strand, W., Bates, S. C., Meehl, G. A., et al. (2018). Predicting near-term changes in the Earth system: A large ensemble of initialized decadal prediction simulations using the Community Earth System Model. *Bulletin of the American Meteorological Society*, *99*(9), 1867–1886. https://doi.org/10.1175/BAMS-D-17-0098.1